Creation of finely focused particle beams from single-component plasmas

T. R. Weber, J. R. Danielson, and C. M. Surko
Department of Physics, University of California at San Diego, La Jolla, California 92093-0319, USA

(Received 6 August 2007; accepted 5 November 2007; published online 16 January 2008)

In a recent communication [Danielson *et al.*, Appl. Phys. Lett. **90**, 081503 (2007)], a nondestructive technique was described to create finely focused beams of electron-mass, charged particles (i.e., electrons or positrons) from single-component plasmas confined in a Penning–Malmberg trap. This paper amplifies and expands upon those results, providing a more complete study of this method of beam formation. A simple model for beam extraction is presented, and an expression for a Gaussian beam profile is derived when the number of extracted beam particles is small. This expression gives a minimum beam diameter of four Debye lengths (full width to $1/e$) and is verified using electron plasmas over a broad range of plasma temperatures and densities. Numerical procedures are outlined to predict the profiles of beams with large numbers of extracted particles. Measured profiles of large beams are found in fair agreement with these predictions. The extraction of over 50% of a trapped plasma into a train of nearly identical beams is demonstrated. Applications and extensions of this technique to create state-of-the-art positron beams are discussed. © *2008 American Institute of Physics*. [DOI: 10.1063/1.2817967]

I. INTRODUCTION

A broad range of science and technology relies upon specially tailored low-energy charged particle beams. Examples include bright beams for microscopy and scattering experiments and cold beams for spectroscopy.[1–5] When copious sources of particles are available, sacrificial techniques can be used to create cold and/or bright beams. However, when the particular particles are scarce, as is the case with antimatter, for example, one must frequently resort to more elaborate, particle-conserving techniques to achieve such goals. As an example, achieving improved spatial resolution by passage through a small aperture is perfectly acceptable for electrons but not for less common particles such as positrons. This motivated the development of a technique to focus and rethermalize a positron beam at a material surface so as to avoid an unacceptably large loss of particles.[6] Here, we describe another technique to create finely focused positron beams with even greater efficiency. Applications include the efficient creation of high-quality positron beams for atomic physics studies and microbeams for material analysis.[1,7,8]

A natural approach to creating tailored positron sources is to accumulate, store, and manipulate these antiparticles in the form of single-component plasmas, thereby keeping them away from matter to avoid annihilation. In this paper, this approach is utilized to demonstrate a nondestructive technique to extract positron beams, with adjustable beam width and brightness, from single-component positron plasmas confined and tailored in a Penning–Malmberg trap.[9] For positron plasmas in this type of trap, infinite storage times are possible, making it a useful device for this purpose. Experiments with electron plasmas (used for increased data rate) are described that demonstrate the utility of this technique. Given that sources of trapped and cooled positrons are readily available, all of the results described here are expected to be valid for positrons without further technical development.[2,10,11] For example, trap based positron beams have already been demonstrated;[12,13] however, the positron density was low enough such that the plasma effects discussed here were negligible.

Shown in Fig. 1 is a schematic diagram of the experimental arrangement.[9] Plasmas are confined radially by a uniform several-tesla magnetic field aligned to the axis of a set of cylindrical electrodes. The end electrodes are biased negatively with respect to the central electrode to confine electrons. Plasmas are cooled by cyclotron radiation. A rotating electric field, created by the application of phased sine waves to a four-segment electrode extending over a portion of the plasma, is used to compress plasmas radially [the so-called "rotating wall" (RW) technique].[14–16] This provides one of the two stages of the spatial focusing. The second stage of focusing, which is the primary subject of this paper, exploits the fact that the potential energy of the particles is largest near the plasma center ($r=0$). Thus, when the confining potential at one end of the plasma is carefully lowered, a beam is formed that is composed only of particles escaping from the region near $r=0$. A spatially localized beam created in this manner is illustrated in Fig. 2 for the case in which a small fraction of the plasma is extracted in a single pulse.

A key result of this paper is that, for sufficiently small beams (i.e., small number of extracted particles), the areal distribution of beam particles deposited on a collector outside the plasma is approximately

$$\sigma_b(r) \approx \sigma_{b0} \exp\left[-\left(\frac{r}{2\lambda_D}\right)^2\right], \tag{1}$$

where $r=0$ is the position of the plasma center and $\lambda_D \propto (T/n_0)^{1/2}$ is the Debye length, with T the plasma temperature and n_0 the equilibrium density.[9] In this work, the beam half-width ρ_b is defined as the half-width to $1/e$ of the distribution; i.e., $\sigma_b(r)$. It will be shown that Eq. (1) is valid

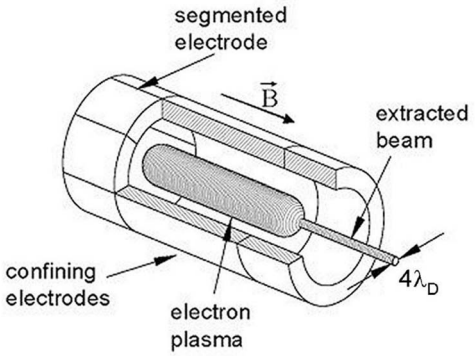

FIG. 1. Schematic diagram of the extraction of a small beam from an electron plasma in a Penning–Malmberg trap equipped with a segmented electrode. For small extracted beams, the beam diameter to $1/e$ is $2\rho_b=4\lambda_D$.

(i.e., $\rho_b=2\lambda_D$) for small beams over a wide range of densities and temperatures.

A beam such as that described by Eq. (1) and illustrated in Fig. 2 is attractive for a wide range of applications. The width, i.e., $2\rho_b$, is a simple function of n_0 and T. By exploiting the ability to nondestructively set these macroscopic parameters *in situ*, the spatial distribution of the beam can be optimized without particle loss (e.g., without aperturing the beam). For example, by increasing n_0 through the application of phased electric fields (the rotating wall technique), the width of beams described by Eq. (1) can be decreased as desired.

This paper expands upon the results presented in a previous communication,[9] providing a more detailed discussion of the beam-formation process. The range of beam width and amplitude for which Eq. (1) is valid is explored, as well as the nature of beams outside of this range. An expression is developed and tested experimentally for larger beams (i.e., larger fractions of the plasma extracted), as well as a numerical method for predicting radial profiles for beams of arbitrarily large fractions of the plasma.

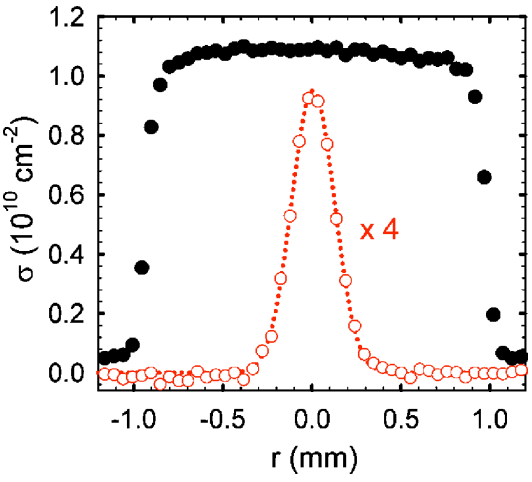

FIG. 2. (Color online) Shown are the radial distribution $\sigma_b(r)$ for a small electron beam (○) and the z-integrated density distribution $\sigma_z(r)$ of the initial plasma (●). Also shown is a Gaussian fit (···) to the beam distribution, which indicates $\rho_b \approx 2.2\lambda_D$.

Also addressed is a problem of paramount significance for beam applications involving scarce particles: Efficiently converting a large fraction of particles in a single plasma into many beams of approximately equal amplitude and width. The process used here is analogous to repeatedly squeezing toothpaste from a tube in small increments as needed. More than half of the plasma can be extracted in this manner with near 100% efficiency. For beam applications, the remainder of the plasma can be left in the trap to be used in the next fill cycle.

This paper is organized as follows. A simple theory of beam extraction is presented in Sec. II. The experimental apparatus and procedures for the studies described here are described in Sec. III. Results for the extraction of single beams are presented in Sec. IV, and results for multiple beams extracted from a single plasma are presented in Sec. V. Applications to positron beams are discussed in Sec. VI. The paper concludes with a set of summary remarks (Sec. VII), including brief comments about areas for future work.

II. THEORETICAL DESCRIPTION OF BEAM EXTRACTION

In this section, expressions are developed for the areal distributions of electron beams extracted from a Penning–Malmberg trap. These results can be applied to positron beams by changing e to $-e$ in the formulae presented below.

The time dependence of the trapping potentials and plasma dynamics make a complete description of the beam extraction process difficult, in principle necessitating a time-dependent calculation.[17] However, the fact that the fastest particles leave the plasma first means the bulk of the plasma tends to be affected only by the value of the plasma potential at the end of the extraction process. Thus, in the description presented here, all time dependence is neglected, and the plasma potential is taken to be that at the end of beam extraction. It is shown below that the predictions obtained using these assumptions are in reasonably good agreement with the results of experiments over a relatively broad range of beam and plasma parameters.

This analysis is analogous to previous work on electron plasmas that used profiles of the extracted charge to measure the plasma temperature (e.g., Refs. 17–20). However, in this paper, a known (measured) plasma temperature is used to calculate the radial profiles of the extracted beams. It is shown that for small beams, the areal distribution of the extracted particles (i.e., the measured charge on a screen or collector plate external to the trap) is approximately a Gaussian with a half-width; i.e., $\rho_b=2\lambda_D$. For larger beams, an approximate analytic relationship is derived relating ρ_b to the number of extracted beam particles N_b.

A long, cylindrical plasma of N_0 particles with radius R_p and length L_p is assumed to be confined in a trap with electrodes of radius R_W, with $R_p \ll R_W \ll L_p$. The change in length is neglected as the confinement potential changes little during beam extraction (typically, $\Delta L_p/L_p < 0.05$). It is assumed that $R_W \ll L_C$, where L_C is the length of the confining electrode, so that the confinement potential V_C is approximately independent of radius. Further, it is assumed that the plasma

is sufficiently cold and/or dense so that $\lambda_D \ll R_p$ and that the plasma is well described as having flat ends. The electrodes surrounding the plasma are grounded, defined as 0 V. Throughout this work, the dependence of potentials and densities along the magnetic field (i.e., the z direction) are neglected, and azimuthal symmetry of the plasma and extracted beams is assumed (i.e., no θ dependence) unless otherwise noted. The plasma is characterized by a single temperature T, taken to be constant during beam extraction, and an initial equilibrium density distribution $n_0(r)$. The initial plasma potential $\phi_0(r)$ is uniquely determined by $n_0(r)$ through the Poisson equation.

For a well-confined plasma, $-eV_C \gg -e\phi_0(0)+T$, where V_C is the confinement potential at the ends of the plasma, and $\phi_0(0)$ is the plasma potential at $r=0$. To extract a beam, V_C at one end of the plasma is raised from −100 V to a value $V_E \sim \phi_0(0)$ for a brief extraction time Δt. A critical assumption in the description here is that the time Δt is sufficiently long so that all the particles that can escape have time to do so, but sufficiently short so that collisions and plasma instabilities do not repopulate the phase space of the exiting particles. A rough lower limit is $\Delta t \geqslant \tau_b \equiv 2L_p/v_t$, where τ_b is the "bounce time" required for an electron with the thermal velocity $v_t=(T/m)^{1/2}$ to travel the distance $2L_p$. The upper limit on Δt is discussed later in this paper. For the data presented here, $\Delta t \approx 10$ μs.

After extraction, the plasma density is reduced to $n(r)=n_0(r)-\Delta n(r)$, where $\Delta n(r)$ is the change in the initial plasma density resulting from the extracted beam. This reduction in density changes the plasma potential to $\phi(r)=\phi_0(r)-\Delta\phi(r)$, where $\Delta\phi(r)$ satisfies the Poisson equation

$$\nabla^2[\Delta\phi(r)] = 4\pi e \Delta n(r). \tag{2}$$

The escape condition for a particle with a parallel velocity $v_\parallel$ is

$$\tfrac{1}{2}mv_\parallel^2 - e[\phi_0(r) - \Delta\phi(r)] \geqslant -eV_E. \tag{3}$$

The areal distribution of the extracted beam, i.e., $\sigma_b(r)=L_p\Delta n(r)$, is the integral over the plasma particles that satisfy Eq. (3),

$$\sigma_b(r) = 2L_p \int_{v_{\min}(r)}^{\infty} f(r,v_\parallel)dv_\parallel = 2L_p n_0(r)\mathrm{erfc}\left(\frac{v_{\min}(r)}{\sqrt{2}v_t}\right), \tag{4}$$

where $f(r,v_\parallel)$ is assumed to be a Maxwellian velocity distribution at temperature T;

$$v_{\min}(r) = \sqrt{-\frac{2e}{m_e}[V_E - \phi_0(r) + \Delta\phi(r)]} \tag{5}$$

is the smallest velocity of escaping particles from Eq. (3); and erfc(x) is the complementary error function with argument $x=v_{\min}/\sqrt{2}v_t$.

For given values of $n_0(r)$ and V_E, Eqs. (2) and (4) can be solved self-consistently using numerical methods to obtain a prediction for the beam profile $\sigma_b(r)$. As will be discussed in Sec. IV, this prediction agrees with the measured values of $\sigma_b(r)$ over a relatively wide range of parameters.

In the small-beam limit, a useful expression for $\sigma_b(r)$ can be obtained analytically. When $x>2$ (i.e., the extracted particles come only from the tail of the Maxwellian), erfc(x) in Eq. (4) can be approximated by[21]

$$\mathrm{erfc}(x) \approx \frac{\exp(-x^2)}{\sqrt{\pi}x}. \tag{6}$$

Assuming an ideal "flat-top" density distribution, i.e., $n_0=[N_0/\pi(R_p)^2L_p]$, the initial space charge potential in the plasma is

$$\phi_0(r) = -\frac{eN_0}{L_p}\left[1 - \frac{r^2}{R_p^2} + 2\ln\left(\frac{R_W}{R_p}\right)\right]. \tag{7}$$

Substituting Eqs. (5)–(7) into Eq. (4) yields

$$\sigma_b(r) \approx \sigma_{b0}\exp\left[-\left(\frac{r}{2\lambda_D}\right)^2\right]\exp\left[\frac{e\Delta\phi(r)}{T}\right], \tag{8}$$

where λ_D is the Debye length of the unperturbed plasma and

$$\sigma_{b0} \approx A\exp\left[\frac{e}{T}[V_E - \phi_0(0)]\right], \tag{9}$$

with A (approximately) a constant. For $|e\Delta\phi/T| \ll 1$, as is the case for a small beam, Eq. (8) becomes

$$\sigma_b(r) \approx \sigma_{b0}\exp\left[-\left(\frac{r}{2\lambda_D}\right)^2\right] \tag{10}$$

[i.e., Eq. (1)]. As discussed above, this areal density $\sigma_b(r)$ is the radial distribution that would be measured when the extracted beam impinges on a collector plate.

Equations (9) and (10) are very useful results. They indicate that, in the small-beam limit, the width of the beam scales with the Debye length and has a value, full width to $1/e$, of $2\rho_b=4\lambda_D$. The amplitude of the beam can be controlled by V_E. However, as more and more charge is extracted from the plasma, $\Delta\phi(r)$ eventually reaches values that cannot be ignored.

In Eq. (8), although the magnitude of $e\Delta\phi/T$ will alter the amount of extracted charge, it is only the variation in $e\Delta\phi/T$ *across the beam profile* that is important in determining the width of the beam. We define the key dimensionless parameter $\xi = e\Delta\phi(\rho_E)/T - e\Delta\phi(0)/T$, where ρ_E is the effective radius of the edge of the beam. Since ξ is determined by the amount of charge in the beam, we approximate $\Delta n(r)$ as a flat-top distribution with total charge N_b and radius ρ_b, to find $\Delta\phi(r) \approx \Delta\phi(0) + (eN_b/L_p)(r/\rho_b)^2$. In this approximation, the beam parameter ξ is

$$\xi \approx \frac{e^2N_b}{TL_p}. \tag{11}$$

Using this result and Eq. (8), the areal density is

$$\sigma_b(r) \approx \sigma_{b0}\exp\left[-\left(\frac{r}{2\lambda_D}\right)^2 + \xi\left(\frac{r}{\rho_b}\right)^2\right], \tag{12}$$

where σ_{b0} contains the radius-independent term arising from $\Delta\phi(0)$. Since ρ_b is defined as the half-width to $1/e$, $\sigma_b(r=\rho_b)=\sigma_{b0}e^{-1}$, the beam width ρ_b is

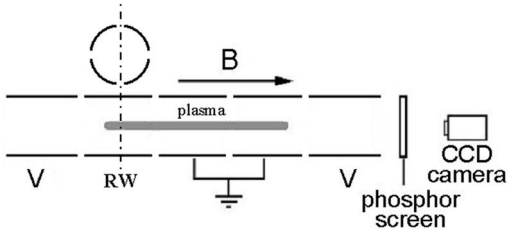

FIG. 3. Schematic diagram of the experimental arrangement.

$$\rho_b \approx 2\lambda_D(1+\xi)^{1/2}. \tag{13}$$

Equations (12) and (13) predict a Gaussian beam, albeit with $\rho_b > 2\lambda_D$, determined by the value of ξ. Thus, the small-beam condition, required for the validity of Eq. (10), can be expressed as $\xi \ll 1$. Since Eq. (11) can also be written as $\xi \approx (N_b/N_0)(R_p/2\lambda_D)^2$, this condition places an important practical constraint on the number of plasma particles that can be extracted in a small beam; namely, $N_b/N_0 \ll (2\lambda_D/R_p)^2$.

Equations (10) and (12) describe well a range of beam profiles observed in experiment. However, when $\xi > 1$, non-Gaussian beam profiles are observed. In this case, numerical solutions of Eqs. (2) and (4) can be used to describe the measured profiles, even when $N_b \sim N_0$.

III. DESCRIPTION OF THE EXPERIMENTS

The Penning–Malmberg trap used for these experiments is shown schematically in Fig. 3. It consists of a series of hollow conducting cylindrical electrodes 0.5 m in total length with radii $R_W = 1.27$ cm. A uniform magnetic field $B = 4.8$ T lies parallel to the electrode axis. For a more complete description of the apparatus (see Ref. 16).

Plasmas are created using a standard electron gun to fill a potential well of variable depth ($V_{\text{fill}} \sim +40$ V). The magnetic field provides radial confinement while axial confinement is achieved by the application of confinement voltages $V_C = -100$ V, to electrodes on either side of the well. The plasma length L_p is roughly the distance between the confining electrodes.

In equilibrium, the plasma has a constant density n_0 (i.e., a flat top radial distribution), and undergoes $E \times B$ rotation at a frequency set by n_0.[16,22] The plasma temperature T is set by the balance between heating sources (due to background drag and/or rotating wall torques) and cyclotron cooling ($\tau_c = 0.16$ s).

Unless otherwise noted, for the plasmas described here, $N_0 = 4 \times 10^8$ electrons, $n_0 = 1 \times 10^9$ cm^{-3}, $R_p = 0.1$ cm, $L_p = 15$ cm, and $T = 0.05$ eV. For these plasmas, the Coulomb collision time $\tau_{ee} < 1$ ms (Ref. 22) is rapid compared to τ_c, thus ensuring that the plasmas are in states of thermal equilibrium where $T = T_\parallel = T_\perp$, independent of position in the plasma. Plasmas exhibit excellent shot-to-shot reproducibility, with $\Delta N_0/N_0 \leqslant 1\%$.

Density and total charge are measured using an aluminum-coated phosphor screen located adjacent to one of the ends of the trap (see Fig. 3). The potential V_C on electrodes at this end of the trap is lowered, and exiting electrons are accelerated into the screen, which is biased at a positive electrical potential. For low screen potentials (e.g., 25 V), the total charge is measured, giving the number of electrons exiting the trap. When V_C is lowered to 0 V; this number is equivalent to N_0. At much higher potentials (e.g., 5 kV), the exiting electrons penetrate the aluminum coating and produce light in the phosphor that is imaged using a CCD camera. When V_C is lowered to 0 V, this image is the two-dimensional (i.e., areal) z-integrated density distribution $\sigma_z(r,\theta)$ of the trapped plasma, where $n(r,\theta) \approx \sigma_z(r,\theta)/L_p$, and is independent of z. For a typical situation described here with rotational symmetry, $\sigma_z(r,\theta)$ is written as $\sigma_z(r)$ with the θ dependence suppressed. Plots of $\sigma_z(r)$ below include values $r < 0$ to represent measurements taken along a major chord through the circular distribution. Measurements of $\sigma_z(r,\theta)$ are shown in Fig. 4, along with the truncated distribution $\sigma_z(r)$.

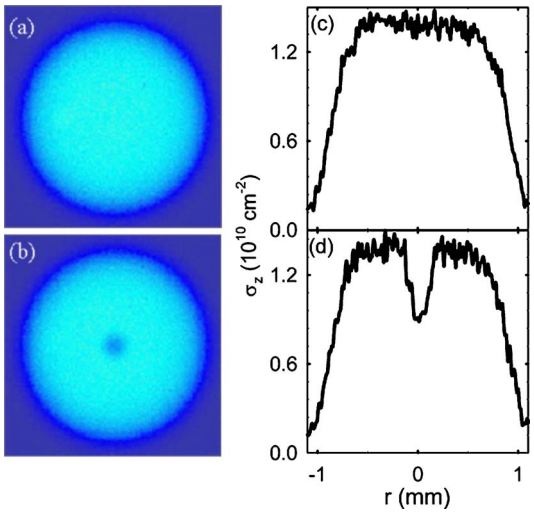

FIG. 4. (Color online) CCD camera images of $\sigma_z(r,\theta)$ for a flat-top plasma (a) before and (b) 10 μs after beam extraction. Shown in (c) and (d) are the corresponding (slice) distributions $\sigma_z(r)$.

The plasma temperature is varied using the technique described in Ref. 18. It consists of repeatedly compressing and expanding the plasma by changing L_p, thereby heating the plasma through Coulomb collisions. The temperature is determined by time-resolved measurement of the number of electrons escaping from the trap while V_C at one end is *slowly* lowered.[19]

The plasma density is varied using the rotating wall (RW) technique.[16,22] Phased sine waves applied to a sectored electrode are used to generate a rotating electric field with azimuthal mode number $m_\theta = 1$. These fields produce a torque on the plasma, thus providing a way to compress or expand the plasma in a nondestructive manner (see Ref. 16 for details).

IV. SINGLE-BEAM EXTRACTION

As discussed above, to extract a beam from the trapped plasma, V_C at one end of the plasma is raised from −100 V to a value $V_E \sim \phi_0(0)$ for a brief extraction time; i.e., $\Delta_t \approx 10$ μs. Using this technique, small beams were extracted

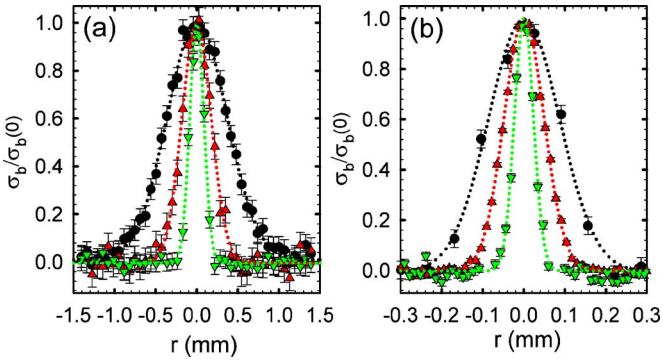

FIG. 5. (Color online) Small-beam profiles $\sigma_b(r)$: (a) $n_0 \approx 1\times10^9$ cm^{-3} and $T\approx1$ eV (●), 0.2 eV (▲), and 0.04 eV (▼). (b) $T\approx0.1$ eV and $n_0\approx1\times10^9$ cm^{-3} (●), 6.5×10^9 cm^{-3} (▲), and 1.2×10^{10} cm^{-3} (▼). Gaussian fits (···) are also shown.

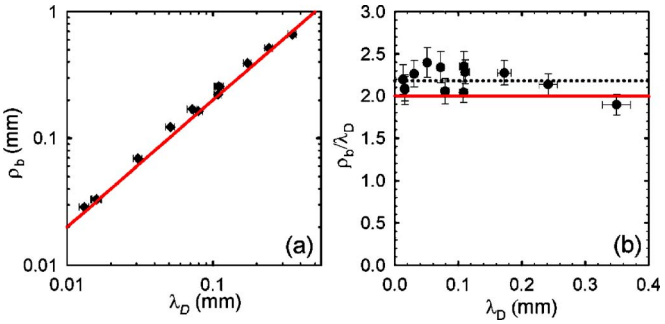

FIG. 6. (Color online) (a) Log-log plot of ρ_b vs λ_D; (b) linear plot of ρ_b/λ_D vs λ_D. The prediction $\rho_b=2\lambda_D$ from Eq. (1) (—) is shown in both (a) and (b). The average, i.e., $\langle\rho_b/\lambda_D\rangle=2.2\pm0.2$, for all data (···) is also shown in (b).

over a factor of approximately 40 in both density ($0.06<n_0<2.2\times10^{10}$ cm^{-3}) and temperature ($0.05<T<2$ eV). Figures 5(a) and 5(b) show examples of $\sigma_b(r)$ and the corresponding Gaussian fits over a range of T and n_0, respectively. However, due to extra heating during RW compression, not all temperatures were achieved at all densities. The observed beam distributions are seen to be in excellent agreement with the Gaussian form of Eq. (1). From the Gaussian fits, the beam half-width ρ_b is found for each extracted beam.

Data for ρ_b over a factor of 30 in λ_D are shown in Fig. 6, and compared with the predictions of Eq. (1). As shown in Fig. 6(b), the average of all the data, i.e., $\langle\rho_b\rangle/\lambda_D=2.2\pm0.2$, is in good agreement with the predicted value of 2.0 in Eq. (1). The small discrepancy between the data and the predictions of Eq. (1) is currently unexplained.

The data in Fig. 5 show that, at constant T, the width of an extracted small beam is determined by λ_D and hence by the plasma density n_0. By varying n_0 in a nondestructive manner with the RW, the width of the extracted beam can be varied *without particle loss*. Profiles exemplifying this are shown in Fig. 7, where n_0 is increased so as to narrow the resulting extracted beam. Here, since $\lambda_D\propto1/\sqrt{n_0}$, as the density is increased by a factor of 4, the measured beam width drops by a factor of 2.

As mentioned above, Eq. (1) is valid only for $N_b\ll N_0(2\lambda_D/R_p)^2$ (i.e., $\xi\ll1$). If N_b exceeds this limit, the extracted beams may exhibit radial distributions that are no longer well characterized by Eq. (1). Experimentally, as N_b is increased to intermediate values, i.e., $0.5<\xi<1$, the beams remain Gaussian, but now $\rho_b>2\lambda_D$ [c.f. Eq. (13)]. As N_b is increased further (i.e., $\xi>1$), the profiles evolve to flat-tops, with steep edges and flat maxima that are no longer well described by Eqs. (12) and (13).

Beam profiles measured over the entire range of N_b from plasmas with the same density ($n_0\approx1\times10^9$ cm^{-3}) but different temperatures are shown in Figs. 8(a) and 8(b) along with the theoretical predictions. For the three smallest beams, the predictions of Eq. (1) are plotted as dotted lines, showing excellent agreement with the measured profiles. For the three larger beams, predictions are obtained by numerically solving Eqs. (2) and (4) using the measured values for $n_0(r)$, T, L_p, and N_b. These predictions, shown as solid lines in Fig. 8, are in reasonable agreement with the measurements, demonstrating that the profile of an arbitrary sized beam, i.e., all beams such that $0<N_b\leqslant N_0$, can be predicted numerically. It is important to point out that beams of any $N_b\leqslant N_0$, can be extracted without exciting plasma instabilities *during* the relatively short extraction time ($\Delta t\approx10$ μs). The stability of the plasma after extraction is discussed later in this section.

From the data shown in Fig. 8, the beam half-width ρ_b can be obtained over a broad range in N_b. Figure 9 shows the results of these measurements together with the predictions of Eq. (13) and numerical solutions to Eqs. (2) and (4). The measured values of ρ_b are in good agreement with the predictions of Eq. (13) with no fitted parameters. Remarkably, agreement is seen over the full range of N_b. As mentioned above, this is not expected for $N_b>0.5N_0$, since the beam profiles depart from the Gaussian shapes predicted by Eqs. (12) and (13). Thus, the agreement with Eq. (13) shown in Fig. 9 may be fortuitous. The beam width predicted by the numerical solutions is in similar agreement with the data. This is expected, as no assumptions on N_b were made in those calculations.

For all beams investigated, the time evolution of the number of particles striking the collector plate per unit time [i.e., the beam current $I(t)$] generally resembles an asymmetric triangle, as shown in Fig. 10. The time dependence of $I(t)$ is of interest, for example, in applications where pulses with a short time duration are required. However, in other appli-

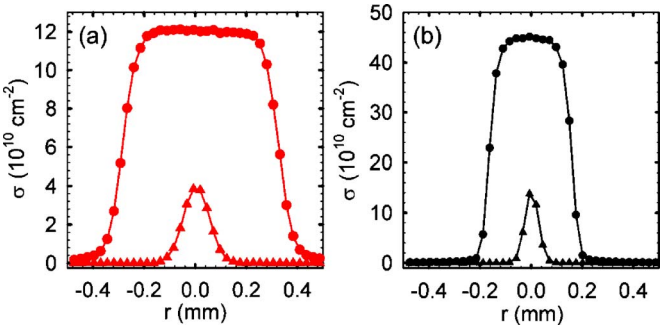

FIG. 7. (Color online) Radial distributions $\sigma_b(r)$ (▲), for beams extracted from a plasma (a) before ($n_0=0.65\times10^{10}$ cm^{-3}) and (b) after RW compression ($n_0=2.2\times10^{10}$ cm^{-3}). The initial plasma profiles $\sigma_z(r)$ (●) are also shown. Here, $L_p\approx22$ cm and $T\approx0.1$ eV.

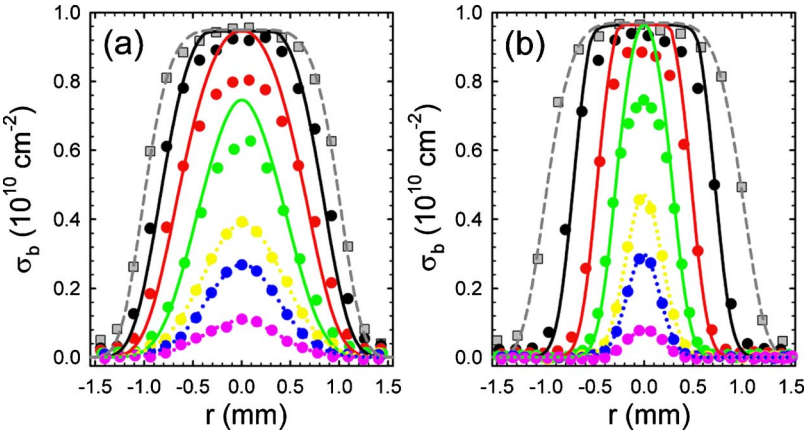

FIG. 8. (Color online) Profiles $\sigma_b(r)$ of extracted beams: (a) $T \approx 1.0$ eV, $\xi \approx 0.1, 0.3, 0.5, 1.0, 1.9, 2.8$; (b) $T \approx 0.2$ eV, $\xi \approx 0.1, 0.3, 0.5, 2.2, 5.2, 11$. In both (a) and (b), the three smallest beams are fit (···) to Eq. (1), and the three largest beams are fit (—) to numerical solutions to Eqs. (2) and (4). The initial plasma profile $\sigma_z(r)$ is shown (□), as is the fit (- - -) used in the numerical solutions.

cations (e.g., scattering, discussed below), the time dependence of the beam pulse is not important. The beam extraction procedure described here produces beams that exit the trap with an initial temporal width Δt_0, roughly equal to the bounce time of a typical escaping particle (i.e., $\Delta t_0 \sim \tau_b$ for exiting particle with energies $\sim 2T$). For the beams described here, $\Delta t_0 \leqslant 1$ μs. Because these beams contain particles with a relatively broad spread in velocities, the pulse width will increase as the beam travels away from the trap. This is likely the dominant effect responsible for the duration of the pulse shown in Fig. 10.

The extraction of multiple beams from the same plasma is an important practical goal (discussed in Sec. V). This is most easily accomplished if the plasma returns to equilibrium after each extraction. To investigate this issue, the plasma response following a single-beam extraction was investigated by recording the areal plasma density $\sigma_z(r)$ at discrete time intervals after the extraction of a small beam. Four such distributions are shown in Fig. 11.

Shortly after the extraction and at $t = 100$ μs, the profile is the initial flat-top profile with a "hole" where the extracted beam particles were removed. By 250 μs, the hole has moved away from the plasma center, breaking the typical θ symmetry in $\sigma_b(r, \theta)$. From the time evolution of $\sigma_b(r, \theta)$ (not shown), the density hole is seen to rotate around the center axis of the plasma, as well as drift radially outward. Similar dynamics are discussed in Ref. 23, in which a similar density hole was created in an electron plasma and displaced slightly off-axis to produce an unstable diocotron mode. In Ref. 23, the density hole is advected around the plasma center with a radial location that grows exponentially with time, analogous to the scenario illustrated in Fig. 11. However, here there is no initial off-axis displacement of the density hole, and so the radial displacement does not reach significant amplitudes until times >100 μs.

Beneficially, this instability does not interfere with the beam extraction process, which occurs in less than 10 μs. Additionally, the instability for small beams, similar to the case shown in Fig. 11, decreases the plasma recovery time, thereby aiding in the extraction of multiple beams. In Fig. 11, the plasma returns to a flat-top state after only 500 μs, much quicker than it would by viscous transport alone. However, for large beams (i.e., $\xi > 1$), other types of plasma instabilities occur (in times >100 μs) that increase the plasma re-equilibration time, and in some cases, prevent the plasma from returning to a flat-top equilibrium state.

These results indicate that, for appropriate sized beams, extraction times as long as 100 μs are possible (assuming collisional effects are negligible) without violating the assumptions of Sec. II. This is verified in Fig. 12, where N_b is plotted for beams extracted on two times scales: The typical 10 μs extraction, and a longer extraction over ~ 200 μs. The

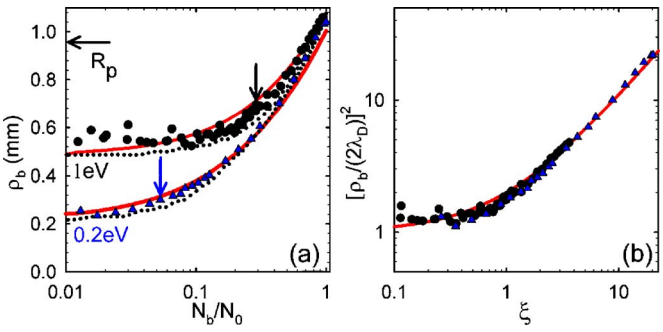

FIG. 9. (Color online) (a) Beam-width parameter ρ_b plotted vs N_b/N_0 for $T \approx 1.0$ eV (●) and 0.2 eV (▲). Predictions (—) from Eq. (13) with no fitted parameters, and (···) numerical solutions to Eqs. (2) and (4). Arrows correspond to beams with $\xi = 1$. (b) Data from (a) plotted as $(\rho_b/2\lambda_D)^2$ vs ξ, showing all data lies on a single curve (—) given by Eq. (13).

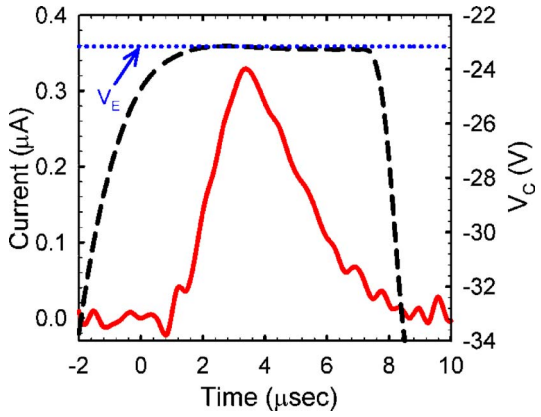

FIG. 10. (Color online) The extracted beam current $I(t)$ (—) for a typical beam is shown together with the time dependence of the confinement potential $V_C(t)$ (- - -). The value of V_E (···) for this extraction is also shown. In this example, $L_p \approx 15$ cm and $\tau_b \approx 3$ μs.

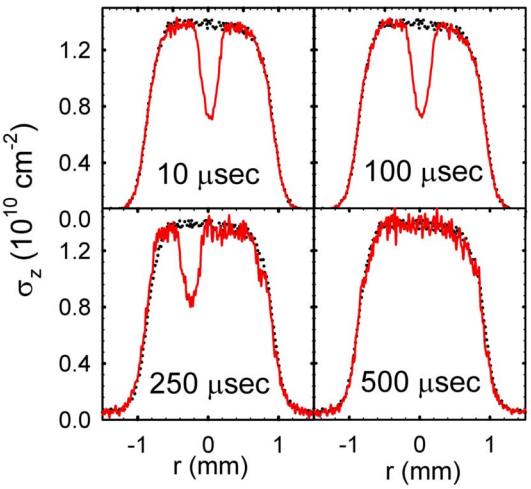

FIG. 11. (Color online) Profiles $\sigma_z(r)$ are shown at four times after the extraction of a small beam. For the data at 250 μs, the major chord along which $\sigma_z(r)$ is measured is chosen to pass through the center of the off-axis hole. Also shown $(\cdots)$ is $\sigma_z(r)$ before the extraction.

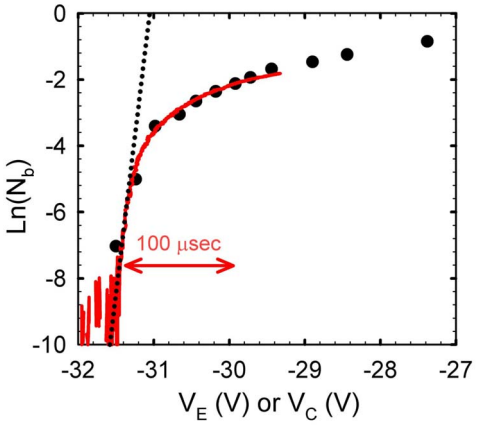

FIG. 12. (Color online) Fast and slow beam extraction procedures are compared: $\ln(N_b)$ (●) for fast ($\sim$10 μs) extractions at different values of V_E; $\ln(N_b)$ (—) vs V_C, as measured continuously while V_C is ramped slowly from -100 V$\rightarrow$0 V at a rate of 0.015 V/μs. Also shown $(\cdots)$ is the prediction in Eq. (9) with T=0.05 eV.

long time scale extraction is performed by a linear ramp of V_C from -100 V$\rightarrow$0 V at a rate of 0.015 V/μs. In this "slow" extraction, unlike the normal beam extraction, both V_C (equivalent to V_E) and N_b are measured continuously as a function of time. As seen in Fig. 12, the two methods extract identical size beams when $V_C=V_E$. This, in turn, provides evidence that no significant radial transport or collisions occur during the longer extraction time. The smooth increase in N_b over the first 100 μs of the slow ramp (indicated by the arrow in Fig. 12), further illustrates the stability of the plasma on these time scales. As shown in Fig. 12, the small N_b part of the slow extraction data can be fit to an exponential [i.e., Eq. (9)] and is used to measure plasma temperatures in the present work.[18,19]

V. EXTRACTION OF MULTIPLE BEAMS

For practical applications, it is desirable to make efficient use of the plasma particles by extracting multiple beams before refilling the trap. One way to do this is to extract a beam at V_E; wait for the plasma to reach a new equilibrium; then extract another beam at $V_E+\Delta V_E$, where $\Delta V_E \approx \Delta\phi_0(0)$, the difference in equilibrium plasma potentials before and after extraction. The adjustment in V_E after each extraction is necessary to maintain constant N_b with changing $\phi_0(0)$ [cf. Eq. (9)]. Although ΔV_E is approximated above, the exact value must be determined empirically. For the multiple beam extractions described below, it was determined that, for constant amplitude pulses, ΔV_E remained invariant throughout the extraction process.

In general, as particles from the plasma are depleted, the plasma density drops, resulting in an increased Debye length. Thus, the later beams would have a larger beam width than the first beams. To counter this effect, we utilize the RW technique (described in Sec. III) to maintain the plasma at a constant density.

Shown in Figs. 13–15 is an example in which about 50% of the plasma was removed by extracting a sequence of 20 beams, while maintaining fixed n_0 with RW compression. In this case, n_0 is held constant while R_p is allowed to vary with each extraction. Actually, n_0 does vary, but only slightly, due to the small amount of "slip" (i.e., $f_{\mathrm{RW}}-f_E \ll f_{\mathrm{RW}}$) that occurs during RW compression.[18]

The total collected charge for each extracted beam is shown in Fig. 13. The time interval between beam extractions was set to 200 ms in order to allow full RW compression after each extraction. Here, this process yielded 20 constant-amplitude beams (i.e., $\Delta N_b/N_b<0.05$), with $N_b \approx 1\times10^7$ per pulse.

In Fig. 14, the z-integrated plasma density is shown before any beam extraction, and after extraction of the 20 beams at fixed $n_0 \approx 2\times10^9$ cm^{-3} and $T\approx0.3$ eV (the density and temperature change by less than 10% over the total extraction) in Fig. 13. Here the RW plasma compression is done at a constant frequency $f_{\mathrm{RW}}=1.05$ MHz, and amplitude $V_{\mathrm{RW}}=1.2$ V. For this case, both n_0 and T (and hence λ_{D}) are approximately constant during the multiple-beam extraction process, while the total number of particles in the plasma drops from $N_{0\mathrm{i}} \approx 4.6\times10^8$ to $N_{0\mathrm{f}} \approx 2.4\times10^8$, corresponding to ejecting 48% of the plasma.

Because the Debye length is the same for each beam, we expect the beam widths to also be the same. This is verified in Fig. 15, where the profiles for the first, tenth, and twentieth extracted beams from Fig. 13 are shown. Here, the measured width ($2\rho_b \approx 0.4$ mm) remains approximately constant for all beams. Using the measured values for n_0, T, L_p, and N, we find $\lambda_{\mathrm{D}} \approx 0.09$ mm and $\xi \approx 0.2$. Plugging these values into Eq. (12), we would expect a beam width $\approx$0.39 mm, in excellent agreement with the measurements.

It should be noted that a previous experiment with positrons in a Penning–Malmberg trap demonstrated multiple beams from a single trapped plasma.[12,13] However, the positron density was low enough (i.e., $\lambda_{\mathrm{D}}/R_p>1$) that no plasma effects (e.g., focusing) were observed. Further, the

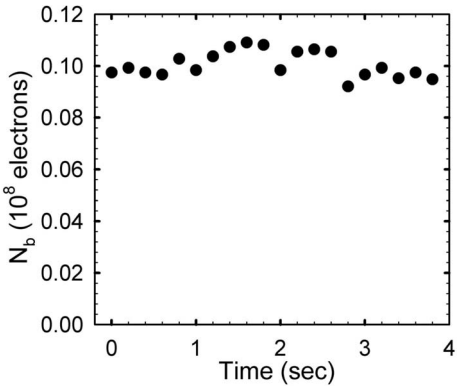

FIG. 13. N_b for 20 electron beams extracted consecutively with $\langle N_b \rangle = (0.1 \pm 0.005) \times 10^8$, with $\xi \approx 0.2$.

time between pulses was much shorter than the re-equilibration time, and thus the plasma distribution was likely non-Maxwellian for all but the first couple of beams. One effect of this was that a nonconstant ΔV_E was necessary in order to produce equal-strength beams.[13] In contrast, the experiments shown here (i.e., Figs. 13–15) demonstrate how a suitable plasma (i.e., $\lambda_D / R_p \ll 1$) can be used to extract more than half the plasma into a series of *identical* beams using a constant ΔV_E.

VI. APPLICATION TO LOW-ENERGY POSITRON BEAMS

A. Magnetically guided beams

One application of the techniques described here is to create cold, bright, low-energy positron beams. Uses include positron microscopy for materials studies,[1] positron spectroscopy of atoms and molecules to study positron-matter interactions,[24] and the creation of dense positron plasmas at material surfaces to create positronium molecules (Ps_2) and Bose-condensed positronium.[25]

One measure of the quality of such beams is the invariant emittance ϵ', which can be approximated as

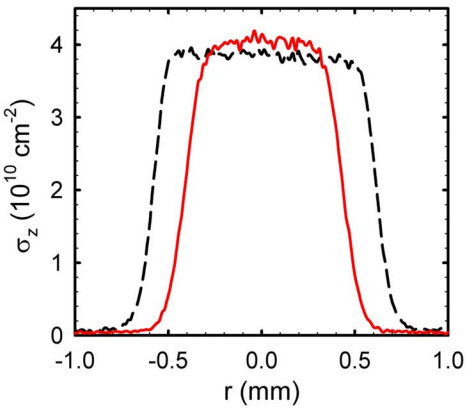

FIG. 14. (Color online) Plasma profiles $\sigma_z(r)$ before (- - -) and after (—) the extraction of 20 beams of $N_b \approx 0.1 \times 10^8$. RW compression holds the plasma parameters ($T \approx 0.3$ eV, $n_0 \approx 2 \times 10^9$ cm^{-3}) approximately constant, while the total number drops from $N_{0i} \approx 4.6 \times 10^8$ to $N_{0f} \approx 2.4 \times 10^8$. Here, $L_p \approx 21$ cm.

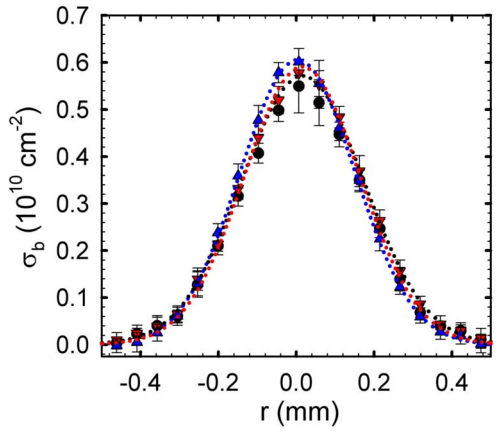

FIG. 15. (Color online) Profiles $\sigma_b(r)$ for the first (●), tenth (▲), and twentieth (▼) extracted beams in Fig. 13. $N_b \approx 0.1 \times 10^8$ for all beams. The beam width ($2\rho_b \approx 0.4$ mm) remains approximately constant, since here λ_D is invariant during extraction. Gaussian fits (···) are also shown.

$$\epsilon' \cong \rho_b (\Delta E_\perp)^{1/2} + [\rho_b^2 / 2 r_c] (\Delta E_\perp)^{1/2}, \tag{14}$$

where $\Delta E_\perp$ is the perpendicular energy spread and r_c the particle gyroradius.[26,27] The two terms on the right-hand side of Eq. (14) correspond, respectively, to the emittance in the electrostatic and strongly magnetized beam limits. In particular, the presence of a magnetic field is deleterious, since ϵ' in this regime is larger by a factor $\rho_b / 2 r_c \gg 1$. Small values of ϵ' correspond to high-quality beams with small spatial extent and angular spread. In the small-beam limit in which $\rho_b \approx 2\lambda_D$,

$$\begin{aligned} \epsilon' &\approx 2 (\Delta E_\perp)^{1/2} \lambda_D + 2 (\Delta E_\perp)^{1/2} (\lambda_D^2 / r_c) \\ &\propto g T n^{-1/2} + h T^{3/2} B n^{-1}, \end{aligned} \tag{15}$$

where g and h are constants. Thus, the emittance can be reduced by reducing T and increasing n, while the presence of the magnetic field always increases ϵ', thereby degrading beam quality. Compression using the RW technique can be used very effectively to increase n, thereby decreasing ϵ'.

In the case of positron scattering experiments, a high premium is placed on beams with small values of energy spread (e.g., Ref. 24). An interesting feature of the beam extraction process described here is that the perturbation of the space charge potential due to the extraction of beam particles acts to retard the extraction. While this has the deleterious consequence of broadening the spatial profile of the beam, it is also beneficial in that it tends to maintain a narrow parallel energy spread, namely, $\Delta E_\parallel \leqslant T$ for extracted beam pulses somewhat beyond the small-beam limit. Although this will also increase the temporal width of the beam pulse (as discussed in Sec. IV), the scattering experiments will not be affected adversely.

B. Electrostatic beams

Thus far, we have discussed magnetically guided beams, since they are naturally compatible with Penning–Malmberg traps. However, electrostatically guided beams are advantageous for a number of applications. For example, they provide increased sensitivity in studying angular scattering from

atomic and molecular targets,[24,28] including the longer-term possibility of developing a positron reaction microscope.[29] One can also use electrostatic techniques for additional beam focusing[6,27] for applications such as Ps_2 and Ps–Bose–Einstein-condensate formation.[30]

Conversion to an electrostatic beam can be done by first transporting the beam adiabatically to a low-field region, then extracting the beam from the field nonadiabatically. The extraction can be accomplished by passing the beam through an aperture, grid, or spokelike structure made of a material with a large magnetic permeability, as long as it is done in a time less than $\sim 1/\omega_c$ (i.e., $\leqslant$ a gyroperiod in the field from which the beam is extracted).[31,32]

Consider, for example, a beam of initial width $\rho_b = 2\lambda_D$ that has been extracted (stage I) from a 30 K (i.e., 3 meV) plasma with density $n_0 = 3\times 10^{10}\ \mathrm{cm}^{-3}$ in a field of $B = 4.8$ T. The corresponding values of ρ_b and ϵ' are $\rho_b = 5\times 10^{-4}$ cm and $\epsilon' = 3\times 10^{-3}\ \mathrm{cm\,eV}^{1/2}$. The beam is then transported adiabatically to a lower field region at $B = 5\times 10^{-4}$ T (stage II), and finally extracted nonadiabatically from the field (stage III) through an aperture of diameter ρ_b that is made from material with a high magnetic permeability. During these processes, ϵ' remains constant. Thus, the final perpendicular energy spread is given by the first term in Eq. (15) (i.e., $B=0$), which yields $\Delta E_\perp \sim 3$ meV. Beam parameters in the three stages of this process are summarized in Table I.

For the example shown in Table I, the resulting electrostatic beam has parallel and perpendicular energy spreads $\leqslant 6$ meV and a diameter $D = 0.1$ cm. The resulting beam would be superb compared to the best electrostatic positron beams currently in use for atomic physics studies,[24] and would admit to further electrostatic brightness enhancement.[6] According to Eq. (13), a beam of this width would be limited in amplitude to $N_b \leqslant 4000$ per pulse.

The final value of $\Delta E_\perp$ could be further reduced using a grid or spokelike structure of high permeability material rather than an aperture for the extraction II→III. In this case, $\Delta E_\perp$ can be estimated by computing the transverse velocity increase $\Delta v_\perp$ that a particle experiences as it moves through the diverging magnetic field at the termination. In CGS units, for a rectangular grid with openings of dimensions $d \ll b$, $\Delta v_\perp \sim \omega_c d$,[31] resulting in a perpendicular energy spread, i.e., $\Delta E_\perp \sim (m/2)(\omega_c d)^2$, where ω_c is the cyclotron frequency. Comparison with Eq. (14) indicates that $\Delta E_\perp$ is further reduced from the aperture-extraction example by a factor of $(d/\rho_b)^2$.

C. Large-amplitude and fast pulses

For many applications, one would also like to have large numbers of positrons per pulse (e.g., creation of Ps_2 and Bose-condensed Ps). Unfortunately, off-the-centerline extraction is not well suited to such tasks. In the small-beam limit, the fraction of extracted particles $N_b/N_0 \ll (2\lambda_D/R_p)^2 < 1$. Rotating wall compression can aid in producing bright pulses with larger numbers of positrons, but off-the-centerline extraction cannot. The latter technique is useful in cases where one wants a train of modest-sized, but cold, bright pulses of particles.

TABLE I. Parameters of a beam extracted from a high-field trap (I), then transported to a low field (II), and finally extracted from the field to create an electrostatic beam (III).

Stage	I	II	III
B (T)	4.8	5×10^{-4}	0
$\Delta E_\parallel$ (meV)	$\leqslant 3$	6	6
$\Delta E_\perp$ (meV)	3	3×10^{-4}	3
ρ_b (cm)	5×10^{-4}	5×10^{-2}	5×10^{-2}

For other applications, such as positron lifetime spectroscopy, one would like short bursts of positrons (e.g., $\Delta t \leqslant 200$ ps).[33] As discussed above, the techniques described here to make cold beams are not well suited to such applications, since the duration of the pulse is limited by the thermal velocities of the particles to times ~ 1 μs for plasmas with temperatures $\leqslant 1$ eV.

VII. CONCLUDING REMARKS

In this paper, we have described new procedures to extract beams with small transverse spatial widths from single-component plasmas. A simple model is presented that predicts the beam profiles. The results are in very good agreement for small beams and in fair-to-good agreement for large beam profiles. Small beams are accurately described by Gaussian radial profiles with a $1/e$ half-width of $2\lambda_D$, as predicted by approximations to the model. Increases in beam width with increasing N_b are predicted analytically by approximations to the model. For larger beams, profiles are predicted from numerical solutions to the simple model for beam extraction.

The ability to control beam widths was demonstrated using rotating electric fields to compress the plasma during the beam extraction process. Furthermore, the ability to convert more than half of the plasma into a train of tailored beam pulses was demonstrated with near 100% efficiency. During this multiple beam extraction, active plasma compression was used to achieve identical width beams, with amplitudes constant to within $\Delta N_b/N_b < 0.05$.

The model used here to describe the extracted beams makes two rather sweeping assumptions. One is that there is no scattering of the particles during the time of extraction. The second assumption is that the radial profile of the plasma potential used to calculate the beam profile is only that *at the end* of the extraction process. Essentially all dynamics (i.e., both of the beam particles and the plasma parameters) during the extraction process are neglected. While the resulting simple model is in reasonable-to-good agreement with the results of experiments over a relatively broad range of plasma parameters, there are important ranges of parameters for which more detailed (time-dependent) calculations would be beneficial. One example is calculation of radial beam profiles for $\xi > 2$ (cf. Figs. 8). Also of interest is the regime of high densities and low temperatures in which the collisional

mean free path of the extracted particles is smaller than the plasma length.

ACKNOWLEDGMENTS

We wish to acknowledge helpful conversations with R. G. Greaves and the expert technical assistance of E. A. Jerzewski. This work was supported by the NSF, Grant Nos. PHY 03-54653 and PHY 07-13958.

[1] A. David, G. Kogel, P. Sperr, and W. Triftshäuser, Phys. Rev. Lett. **87**, 067402 (2001).
[2] C. M. Surko and R. G. Greaves, Phys. Plasmas **11**, 2333 (2004).
[3] Y. Yamazaki, Mater. Sci. Forum **445–446**, 430 (2004).
[4] W. E. King, G. H. Campbell, A. Frank, B. Reed, J. F. Schmerge, B. J. Siwick, B. C. Stuart, and P. M. Weber, J. Appl. Phys. **97**, 111101 (2005).
[5] P. Hommelhoff, Y. Sortais, A. Aghajani-Talesh, and M. A. Kasevich, Phys. Rev. Lett. **96**, 077401 (2006).
[6] A. P. Mills, Jr., Appl. Phys. **23**, 189 (1980).
[7] A. P. Mills, Jr., Science **218**, 335 (1982).
[8] P. J. Schultz and K. G. Lynn, Rev. Mod. Phys. **60**, 701 (1988).
[9] J. R. Danielson, T. R. Weber, and C. M. Surko, Appl. Phys. Lett. **90**, 081503 (2007).
[10] R. G. Greaves and J. Moxom, in *Non-Neutral Plasma Physics V*, edited by M. Schauer, T. Mitchell, and R. Nebel (American Institute of Physics, Melville, 2003), p. 140.
[11] L. V. Jorgensen, M. Amoretti, G. Bonomi *et al.*, Phys. Rev. Lett. **95**, 025002 (2005).
[12] S. J. Gilbert, C. Kurz, R. G. Greaves, and C. M. Surko, Appl. Phys. Lett. **70**, 1944 (1997).
[13] C. Kurz, S. J. Gilbert, R. G. Greaves, and C. M. Surko, Nucl. Instrum. Methods Phys. Res. B **143**, 188 (1998).
[14] X. P. Huang, F. Anderegg, E. M. Hollmann, C. F. Driscoll, and T. M. O'Neil, Phys. Rev. Lett. **78**, 875 (1997).
[15] E. M. Hollmann, F. Anderegg, and C. F. Driscoll, Phys. Plasmas **7**, 2776 (2000).
[16] J. R. Danielson and C. M. Surko, Phys. Plasmas **13**, 055706 (2006).
[17] G. W. Hart and B. G. Peterson, Phys. Plasmas **13**, 022101 (2006).
[18] B. R. Beck, J. Fajans, and J. H. Malmberg, Phys. Plasmas **3**, 1250 (1996).
[19] D. L. Eggleston, C. F. Driscoll, B. R. Beck, A. W. Hyatt, and J. H. Malmberg, Phys. Fluids B **4**, 3432 (1992).
[20] J. Aoki, Y. Kiwamoto, and Y. Kawai, Phys. Plasmas **13**, 112109 (2006).
[21] M. Abromowitz and I. A. Stegun, *Handbook of Mathematical Functions* (Dover, New York, 1964).
[22] J. R. Danielson and C. M. Surko, Phys. Rev. Lett. **95**, 035001 (2005).
[23] C. F. Driscoll, Phys. Rev. Lett. **64**, 645 (1990).
[24] C. M. Surko, G. F. Gribakin, and S. J. Buckman, J. Phys. B **38**, R57 (2005).
[25] D. B. Cassidy, S. H. M. Deng, R. G. Greaves, T. Maruo, N. Nishiyama, J. B. Snyder, H. K. M. Tanaka, and A. P. Mills, Jr., Phys. Rev. Lett. **95**, 195006 (2005).
[26] F. J. Mulligan and M. S. Lubell, Meas. Sci. Technol. **4**, 197 (1993).
[27] R. G. Greaves and C. M. Surko, Nucl. Instrum. Methods Phys. Res. B **192**, 90 (2002).
[28] W. E. Kauppila and T. S. Stein, Adv. At., Mol., Opt. Phys. **26**, 1 (1990).
[29] J. Ullrich, R. Moshammer, A. Dorn, R. Dörner, L. Ph. H. Schmidt, and H. Schmidt-Böcking, Rep. Prog. Phys. **66**, 1463 (2003).
[30] A. P. Mills, Jr., D. B. Cassidy, and R. G. Greaves, Mater. Sci. Forum **445–446**, 424 (2004).
[31] M. Shi, D. Gerola, W. B. Waeber, and U. Zimmermann, Appl. Surf. Sci. **85**, 143 (1995).
[32] D. Gerola, W. B. Waeber, M. Shi, and S. J. Wang, Rev. Sci. Instrum. **66**, 3819 (1995).
[33] R. G. Greaves, S. J. Gilbert, and C. M. Surko, Appl. Surf. Sci. **194**, 56 (2002).